Flooded by Success: On the role of electrode wettability in CO_2 electrolyzers that generate liquid products

McLain E. Leonard[a], Michael J. Orella[a], Nicholas Aiello[a], Antoni Forner-Cuenca[a,b], Yuriy Román-Leshkov[a], and Fikile. R. Brushett[a,*]

[a] Department of Chemical Engineering, Massachusetts Institute of Technology, Cambridge, MA, 02139, USA

[b] Membrane Materials and Processes, Department of Chemical Engineering and Chemistry, Eindhoven University of Technology, Het Kranenveld 14, P.O. Box 513, 5600 MB Eindhoven, The Netherlands

KEYWORDS: wettability, flooding, gas diffusion electrode, electrochemical reduction, carbon dioxide, organic products

*E-mail: brushett@mit.edu, Phone: 617-324-7400

ORCID

McLain E. Leonard: 0000-0003-4572-5251

Michael J. Orella: 0000-0003-1207-4704

Nicholas Aiello: 0000-0002-7507-6937

Antoni Forner-Cuenca: 0000-0002-7681-0435

Yuriy Román-Leshkov: 0000-0002-0025-4233

Fikile R. Brushett: 0000-0002-7361-6637

Abstract

The economic operation of carbon dioxide (CO_2) electrolyzers generating liquid products will likely require high reactant conversions and high product concentrations, conditions anticipated to challenge existing gas diffusion electrodes (GDEs). Notably, electrode wettability will increase as lower surface tension products (e.g., formic acid, methanol, ethanol, and 1-propanol) are introduced into flowing electrolyte streams potentially leading to flooding. To better understand the hydraulically stable electrolyzer operating envelopes in mixed aqueous-organic liquid domains, we connect intrinsic porous electrode wettability descriptors to system operating parameters such as electrolyte flow rate and applied current. Specifically, we first measure contact angles of various water-organic dilutions on polytetrafluoroethylene (PTFE) and graphite surfaces as *ex situ* planar analogues for the major GDE components. We then use material balances around the reactive gas-liquid interface, to calculate product mass fractions as a function of liquid water sweep rate (water source and diluent) and the total current. Product composition maps enable visualization of the extent to which changes in cell performance can lead to changes in capillary pressure, a crucial determinant of GDE saturation. These analyses reveal that formic acid product mixtures pose little risk for GDE flooding across a wide range of flow rate and current combinations, but that effluents enriched with less than 30% alcohols content by mass may cause flooding. This study provides initial guidance into estimating flooding conditions for PTFE-based GDEs in contact with organic-enriched streams and indicates opportunities for oleophobic surface treatments that repel aqueous and organic liquids, expanding regions of stable operation.

1. Industrial CO_2 to liquids electrolyzers will move beyond *differential* operation

Electrochemical carbon dioxide reduction (CO2R) is increasingly recognized as a viable technology for flexible generation of chemicals using carbon dioxide (CO_2) recovered from industrial exhaust streams or directly captured from air [1,2]. When coupled with affordable electricity generated from renewable sources, CO2R has the potential to displace petroleum-based chemicals production in a low-carbon economy [3]. Given that the form factors of electrochemical technologies evolve as they transition from benchtop prototypes in the laboratory to engineered unit operations integrated into an industrial process, it is reasonable to anticipate commensurate shifts in the objectives and challenges for each scale. Historically, three-electrode analytical cells have been used to study catalyst activity, selectivity, and stability with a goal of incorporating proven materials into larger devices [4–6]. However, it has been recognized that the limited CO_2 flux through bulk volumes of liquid electrolyte suppress the reaction rate of CO_2 and inhibit the performance of otherwise promising catalyst systems [7–9]. Gas-fed electrolyzers adapted from commercially successful water electrolyzer and fuel cell technologies have motivated CO2R researchers to explore various combinations of porous electrodes, catalyst layers, liquid electrolytes, and membranes to achieve higher areal productivity while maintaining steady fluxes of species between flow channels and the active sites [10–14]. For example, present art demonstrates that high current density production (> 200 mA cm^{-2}) of valuable intermediates, such as carbon monoxide (CO), at moderate cell voltages (ca. 3 V) and durations (ca. 100 h) is achievable at ambient conditions using cell configurations similar to polymer electrolyte water electrolyzers [15].

At the bench-scale, where component validation and performance benchmarking are typically the desired outcomes, electrochemical cells with active areas of ca. 1–10 cm^2 are often operated with low single-pass CO_2 conversion (< 20%) (**Fig. S1**, Supporting Information), although the definition of low conversion is somewhat arbitrary. At *differential conditions*, reactant conversion as well as concentration, temperature, pressure, and voltages distributions are assumed to be small [16]. By operating reactors in this regime, electrochemical kinetic phenomena can be more clearly characterized in the absence of nonlinear concentration or mass transfer effects that may present at higher degrees of reactant depletion. As an added benefit, such conditions also minimize the

risk of generating toxic reaction products in high concentrations that are more appropriately handled in industrial settings where suitable hazard management protocols exist.

In contrast, the choice of operating conditions and reactor architecture for commercial CO2R systems will be driven by application economics to the point that many of the conditions explored at a bench-scale may not reflect those experienced by practical systems. As an illustrative example of this, we consider a simple case of industrial CO2R with sequential unit operations to first convert the CO_2 feedstock to a crude product and then to separate that stream into a refined product stream for further use or sale, a waste stream for treatment and elimination, and an unreacted material stream for recycle (**Fig. 1a**). We previously introduced a general techno-economic framework for characterizing electrolytic systems, which captures relevant trade-offs between feed concentration, reactant conversion, and separation costs for CO2R [17]. Using this model we can qualitatively show the impact of increasing reactant conversion on the cost of CO2R processes with three different liquid products (formic acid, methanol, and ethanol) (**Fig. 1b**). In each case, increases to reactant conversion decrease separations cost, which outweigh the corresponding increase in concentration overpotential until the mass-transfer limiting-current is met. At this diffusion-limited threshold, additional reactors are necessary to expand system productivity. It should be noted that the definitions of conversion and productivity in this analysis rely on the assumption that no CO_2 is lost to carbonation and no product crossover and re-oxidation occurs at the anode. Based on this coarse analysis, process economics will likely dictate that future at-scale CO2R systems operate at much higher conversions than those contemplated at the laboratory-scale today. This, in turn, may give rise to scientific and engineering challenges that, to date, remain unarticulated. Accordingly, publications focused on scale-up have begun to highlight electrolyzers which operate with high current densities [18], large total currents [19], and, to a lesser extent, enriched product streams [20–22].

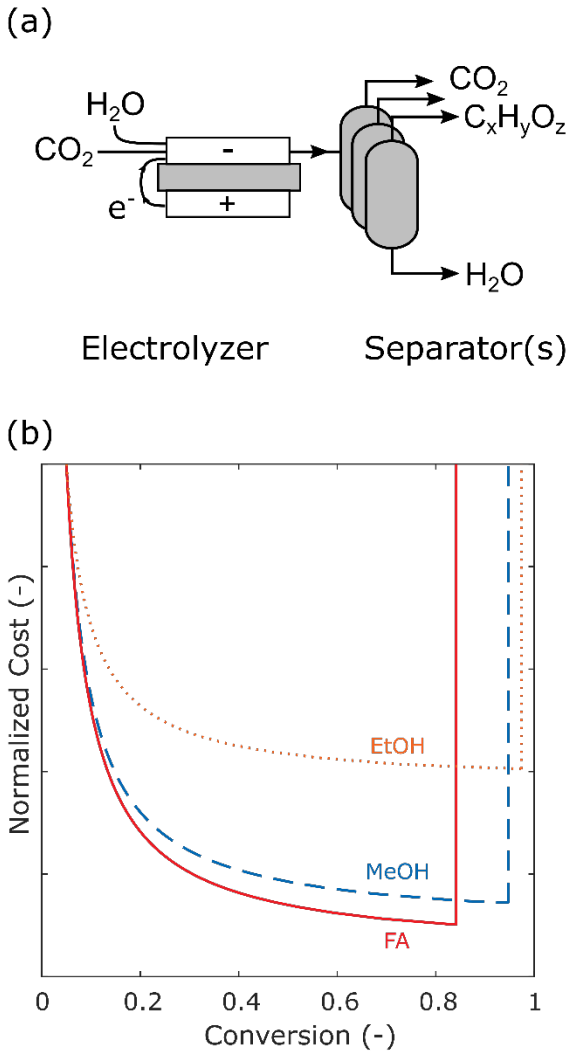

Fig. 1 (a) A general CO2R upgrading scheme involving generic electrolysis and separation blocks. It may be favorable to recycle unreacted CO_2 into the electrolyzer unit step to avoid minimize emissions. (b) Production costs for CO2R products reach lower limits as a function of increasing single-pass conversion. The vertical lines at high conversions represent the abrupt cost increase as the respective processes reach mass transport limiting currents.

As CO2R prototypes begin to traverse these new operating regimes, challenges can be anticipated due to shifts in chemical compatibility requirements for reactor components (catalysts, electrodes, periphery), significant deviations from low-concentration kinetic behavior, and greater process safety concerns arising from concentrated toxic products. Here, we elect to focus on irregularities expected to arise for gas diffusion electrodes (GDEs) during the operation of gas-fed CO2R devices at high conversion and product generation rates as the other topics are more widely studied at present. Recent reports of flowing electrolyte CO2R cells with extended durability (ca. 10–100 h) have generally espoused the importance of incorporating fluorinated polymers (i.e.,

polytetrafluoroethylene (PTFE)) in the GDEs, either as an additive or a structural component, to maintain a stable gas-liquid interface between the liquid product/electrolyte phase and gaseous reactant phase [18,23,24]. This idea has credence given historical uses of fluorinated polymers such as PTFE and fluorinated ethylene propylene (FEP) as *hydro*-phobic *wet-proofing* components in GDEs to assist in water management in fuel cell operations [25] or as a component in oxygen depolarized GDEs for their ability to aid in facile oxygen reduction while maintaining stable gas-electrolyte interfaces [26]. Indeed, initial investigations by Haas *et al.* and Dinh *et al.* would suggest that fluoropolymer-rich GDEs can significantly improve operating lifetimes of a variety of CO2R cell architectures [24,27]. However, we posit that the conditions necessary for industrial CO2R may render GDEs composed of *hydrophobic* materials incompatible with lower-surface-tension mixed aqueous-organic phases generated from the reactive gas-liquid interface.

Expanding on this hypothesis, we first consider the wettability of GDE components, evinced by the sessile drop contact angle on planar analogues, in contact with aqueous-organic liquid mixtures representative of potential product stream compositions. Subsequently, we use a simple mass balance model paired with contact angle measurements to estimate electrolyzer operating limits, represented by the capillary pressure, beyond which product streams would be anticipated to spontaneously flood conventional GDEs without deploying additional pressure control strategies. By connecting readily-obtainable measures of electrode-liquid affinity to cell operating conditions, we aim to develop insights into operating regimes for CO_2 electrolyzers that generate liquid products and to address critical questions such as: (i) Do target effluent compositions fall within stable region for PTFE-based GDEs? (ii) What are crossover compositions for liquid product mixtures that may lead to spontaneous electrode wetting under pressure-balanced conditions? (iii) What is an acceptable gas-liquid pressure difference to maintain optimal saturation of the GDE?

2. Gas diffusion electrode flooding is governed by capillary pressure and wettability

In CO2R, the GDE serves as (i) a scaffold for the catalyst layer and (ii) an interface between the gaseous and liquid phases that facilitates flux of reactants/products/electrons to/from the catalytically active sites. A key challenge is the rational selection of GDE materials that can balance both primary (e.g., electrical conductivity and electrocatalytic activity/selectivity) and secondary (e.g., permeability and chemical compatibility) functionalities across a range of operating modes. Crucially, the stability of the cathode-electrolyte interface is intimately tied to the *wettability* of the GDE, that is captured by the value of the solid-liquid-vapor contact angle, θ. This angle can be used to determine the extent of saturation of idealized cylindrical pores of radius r, with a liquid-vapor surface tension of γ, as measured by the capillary pressure P_C. The Young-Laplace framework (Equation 1) defines the relationship between these variables at equilibrium, where P_C is the difference between the vapor and liquid phase pressures (P_G, P_L)**Error! Reference source not found.** [28].

$$P_C = P_L - P_G = \frac{-2\gamma\cos\theta}{r} \qquad \text{Equation 1}$$

Although quantitatively different from the behavior of real materials due to effects including tortuosity, constrictions, and dead-ends, the parametric trends suggested by Equation 1 remain valid. For the purpose of this preliminary analysis, we ignore any additional complexities that might arise in real materials and instead elect to focus on capillarity trends using simplified cylindrical geometries.

Understanding the effects of material selections on wettability properties of the electrodes requires a comprehension of materials energetics. Electrodes are often combinations of high energy (HE; metal or carbon) materials that readily wet most liquids [29] and low energy (LE; binders or additives) materials used to wet-proof the surfaces. Modifications to electrode surfaces can drastically change wettability characteristics regardless of the bulk material [29]. In the 1960s, pioneering work by Zisman characterized the spreading and adhesion of liquids on solids as a function of surface energy/surface tension [30]. What is evident and readily applicable from the results of Zisman is that (i) macroscopic solid-liquid-vapor (SLV) contact angles track with the

composition of test fluids according to the surface tension and that (ii) solutions transition from non-wetting to wetting at different threshold surface energy values depending on the identity and physical structure of the solid material in question. While PTFE as a GDE support has expanded the envelope for high-current electrolysis, stability at the cathode-electrolyte interface is expected to be perturbed by high concentrations of liquid products such as alcohols, which have also been reported to dissolve anion-exchange membrane materials *in situ* [21].

Commonly pursued CO2R products like organic acids (i.e., formic acid) and C1-C3 primary alcohols (i.e., methanol, ethanol, 1-propanol) are water-miscible at ambient conditions, so even at dilute concentrations, these species can greatly affect physical properties such as density, viscosity, and liquid-vapor (LV) surface tension (**Fig. S2**). Changes to density and viscosity affect pressure drops within flowing electrolyte-based cells; however, we choose not focus on pumping duties for these analyses. Changes to surface tension/contact angle, in combination with electrode geometries, most directly influence GDE wetting and saturation, which acutely impact reactant fluxes and, therefore, electrocatalytic performance. Measuring the *apparent* contact angles of sessile droplets is an effective method for characterizing the wettability of candidate porous electrode materials with a variety of test liquids reminiscent of CO2R product streams. Although this macroscopic approach is often applied to study non-ideal substrates, *intrinsic* contact angles can only be measured on smooth, non-porous surfaces (Young's theory) [31]. Appropriate corrections to contact angles measured on textured materials, which appear distorted when compared to flat materials with equivalent surface chemistry [29], can be made for both homogenous (Wenzel) and heterogeneous (Cassie-Baxter) wetting regimes [32,33]. Despite the obscurations introduced by roughness and entrapped fluids when determining quantitative measures of wettability on porous substrates, droplet based-protocols are widely practiced to qualitatively evaluate the resistance of textiles and other materials to wetting [34,35].

To better our understanding of wettability in aqueous-organic mixtures of compositions similar to, we selected formic acid (FA; reagent grade, ≥ 95% purity, Sigma-Aldrich), methanol (MeOH; HPLC grade, ≥ 99.9%, Sigma-Aldrich), ethanol (EtOH; anhydrous, 200 Proof, KOPTEC), and 1-propanol (PrOH; ACS reagent, ≥ 99.5%) for analysis. We prepared solutions across a range of dilutions from 0 to 100% by mass with deionized (DI) water (18.2 MΩ, Milli-Q). Salt-free solutions were used to isolate the interaction between each test liquid and water. Subsequent

studies may contemplate the impacts of the chemistry and concentration of dissolved salts on relevant physical properties. PTFE (FP303050, Goodfellow) and graphite (99.997%, 867-421-20, Goodfellow) sheets were used as the primary solid substrates for droplet studies. PTFE sheets were cleaned with DI water and isopropyl alcohol (IPA) and dried using compressed air prior to analysis. Graphite sheets were prepared by removing the top layer of material with Scotch® tape (MFR#: 810, 3M). 5-μL droplets were dispensed onto substrates using an automatic pipetting unit. Measurements were taken in ambient air where the temperature and relative humidity remained between 20–24°C and 10–40%, respectively. Videos of 30–60 second duration were captured using a contact angle goniometer system (Model 200, ramé-hart) and processed using DropPy V1.0.0a0, a Python-based goniometer software [36]. Substrates were spot-cleaned before dispensing and imaging new droplets. Contact angles were determined by fitting edges with a two-parameter Bashforth-Adams model that accounts for the effects of gravity on droplet shape. Additional descriptions of experimental procedures (Sections S.1 and S.2) as well as the data collected for each trial (**Tables S1** and **S2**) are provided in the Supporting Information.

To determine the qualitative impact of mixed organic-aqueous product streams on electrode wettability, we measured the contact angles for the solutions described above as a function of water content, as shown in **Fig. 2**. The markers for each product represent the average contact angle from 5 trials at each concentration and the error bars are one standard deviation of the same measurements. As expected, the contact angles of the mixtures on both surfaces decrease with increasing mass fraction of organic species due to the reducing surface tension. The tendency to wet the solids is directly proportional to the carbon chain length of the product which is associated with decreased polarity and surface tension (PrOH < EtOH < MeOH < FA < water), especially for the primary alcohols [37]. The ability for each solid to prevent wetting can be studied by comparing the point at which the test fluid is neutrally wetting, e.g., has a contact angle of 90°. When studying graphite, fluids with more than 10% alcohol fall below the 90°-threshold; however, the alcohols can be mixed in higher proportions before neutrally wetting conditions are reached on PTFE. In both cases, the formic acid mixtures reach neutrally wetting conditions at much greater mass fractions than the alcohols, suggesting that such product streams will not lead to significant changes in capillarity relative to pure aqueous solutions in PTFE-based GDEs. As such, CO2R to FA appears to have a wide range of feasible operating compositions, exceeding the highest reported concentrations to date (ca. 15% by mass) [20]. In contrast, the alcohol crossover

concentrations are significantly lower and we anticipate that such compositions will be readily-achievable in practical CO_2 to liquid electrochemical processes posing a stability challenge for PTFE-based GDEs.

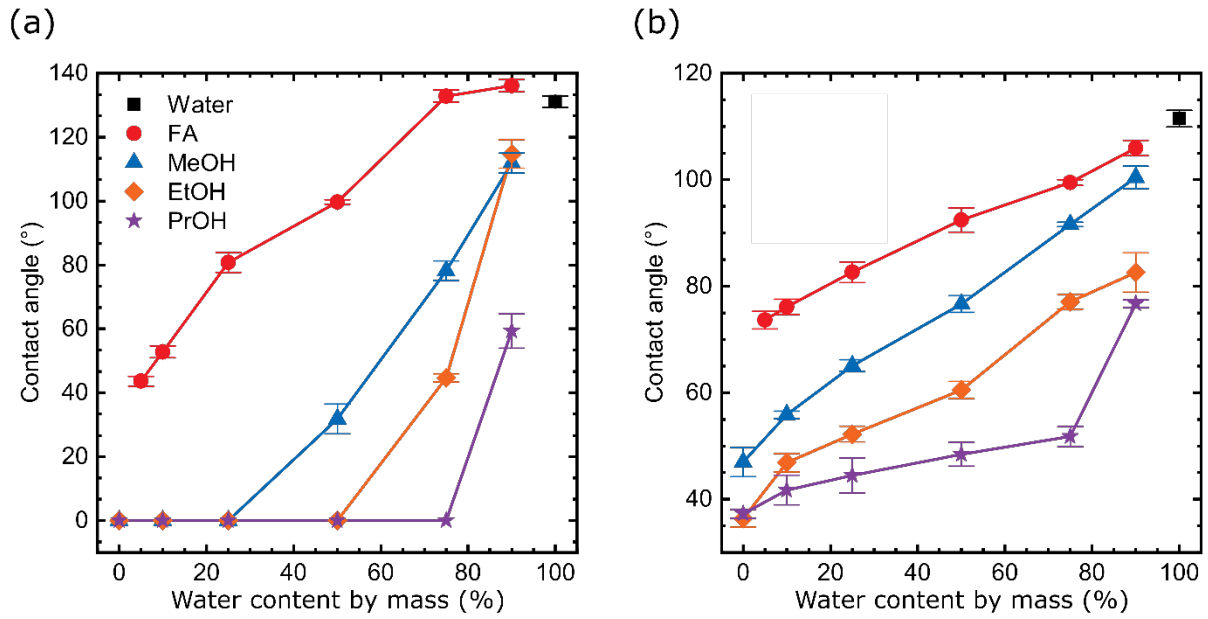

Fig. 2 Sessile drop contact angles on (a) graphite and (b) PTFE for an array of liquid CO2R products as a function of water content by mass.

Beyond experimental measurements of the apparent contact angles of test fluids, γ can be used as a unified predictor for the wettability of different fluid mixtures [29]. With the previous θ measurements, we can construct Zisman plots (**Fig. 3**) to predict the critical surface tension, γ_C, for complete wetting ($\theta = 0°$) and the surface tension at the crossover composition ($\theta = 90°$) for both graphite and PTFE. We fit the data (black open circles) for each surface with quadratic functions (red lines), which is reasonable based on previous analyses that used similar empirical fits [30]. We then predict γ_C values of 31.8 mN/m for graphite (RMSE = 16 mN/m) and 15.2 mN/m for PTFE (RMSE = 7.3 mN/m). We validated this method using a secondary set of test fluids and determined γ_C to be 14.8 mN/m for PTFE. The validation data (**Table S3**) along with an additional Zisman plot (**Fig. S3**) can be found in the Supporting Information. As can be seen for graphite, the data below 31.8 mN/m represent the product compositions that completely spread when contacting the solid. Note that none of the dilutions tested were of sufficiently low surface tensions to reach the critical point for PTFE, so the empirical fit is needed to estimate γ_C. The 90°-crossover

compositions are predicted to be 45 mN/m and 47 mN/m for graphite and PTFE, respectively. These values are useful for predicting sign changes in P_C, as will be considered in the next section. For comparison, Zisman reported a 90°-crossover point of ca. 40 mN/m for PTFE, but did not report a value for graphite, which is reasonable given the wettability of graphite surfaces vary widely depending on form factor [38]. Indeed, identification of smooth, flat material as a representative proxy for carbon particles and/or fibers remains elusive. Qualitatively, the γ_C value predicted for graphite exceeds that of PTFE, which is to be expected as it is the higher energy material.

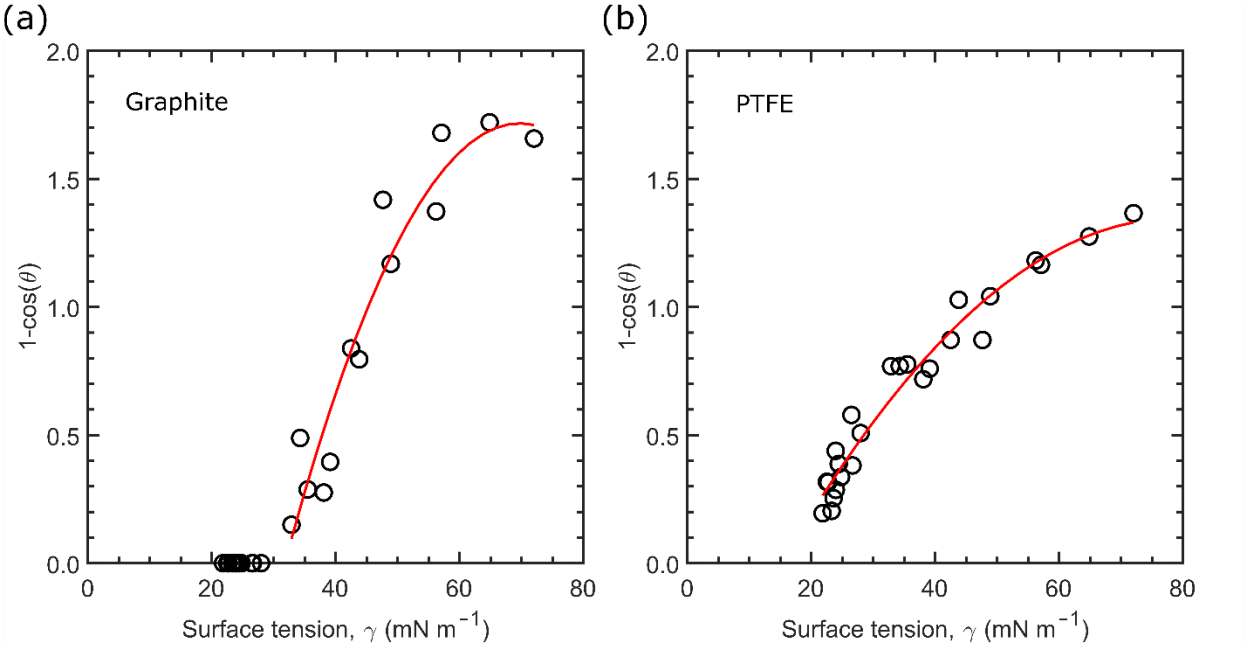

Fig. 3 Zisman plots for (a) graphite and (b) PTFE for all the liquids used to predict critical crossover compositions. Empirical quadratic fits are plotted in red for determining the critical surface tension, γ_C, of each material.

3. Operating envelopes are mapped using electrolysis mass balances

While *ex situ* contact angle data only provide qualitative insights on wettability for porous electrodes, such understanding informs materials selection for different classes of reactions. Here, we use wettability data in combination with a simple mass balance model around the cathode reaction zone to estimate ranges of feasible operating conditions before liquid product enrichment near the gas-liquid interface leads to electrode flooding. A mass balance model represented by the schematic in **Fig. 4** accounts for the mass flow rates of water and organic products to/from a well-mixed flowing liquid phase control volume. The results and possible implications of changing electrolyzer set points are discussed in the context of the widely studied flowing liquid electrolyte configuration [8,10,23,24,27,39–51].

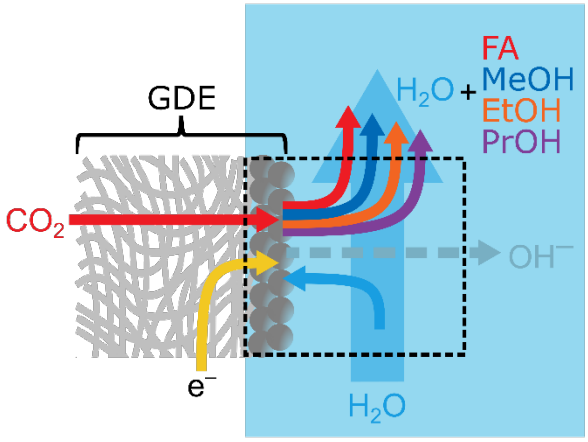

Fig. 4 Electrolyzer mass balance model schematic. Water is fed to the cathode GDE where CO_2, water (H_2O), and electrons (e^-) are consumed within the catalyst layer to produce liquid organic components. The exiting stream contains an aqueous-organic mixture. We do not include the contributions of OH^- and other ions on the overall mass balance or liquid phase properties.

Faraday's law of electrolysis connects the mass flow rates for product generation, $m_{P,rxn}$, (Equation 2) and water consumption, $m_{W,rxn}$, (Equation 3) at the cathode to the current (I) and one of the two stoichiometric coefficients, z_P and z_W, which correspond to the number of electrons per mole of product generated and water consumed, respectively.

$$\dot{m}_{P,rxn} = \frac{I}{z_P F} MW_P \qquad \text{Equation 2}$$

$$\dot{m}_{\mathrm{W,rxn}} = \frac{I}{z_{\mathrm{W}} F} MW_{\mathrm{W}} \qquad \text{Equation 3}$$

In these equations, F is the Faraday constant (96485 C mol e^{-1}) and MW_{P} is the molecular weight of a product species (e.g., g/mol). The molecular weight of water, MW_{W}, is taken to be 18.02 g/mol. The mass flow rate of feed water, $m_{\mathrm{w,in}}$, is defined (Equation 4) as a function of the inlet volumetric sweep rate, Q, and the density of water, ρ_{W}.

$$\dot{m}_{\mathrm{W,in}} = \rho_{\mathrm{W}} Q \qquad \text{Equation 4}$$

Generally, the *sweep rate* of liquid electrolyte impacts product flux away from the catalyst layer to the bulk electrolyte and, by extension, the distribution of product concentrations along the reactor length and at the exit. In this treatment, we select Q directly to regulate product dilution for a given current, but this ability to independently control product removal and tune dilution would be hampered in polymer-electrolyte-based devices as alternative flux mechanisms like evaporation and membrane crossover are less readily controlled [21].

We implement material balances around electrons, water, and liquid reaction products to directly calculate the total mass exiting the reactor, m_{out} (Equation 5), while ignoring dissolved gases (e.g., CO_2, hydrogen, carbon monoxide, etc.) and dissociated ions such as hydroxide (OH^-) produced from the cathodic half-reactions as well as bicarbonate (HCO_3^-) and carbonate (CO_3^{2-}) that form as a result of carbonation reactions [52].

$$\dot{m}_{\mathrm{out}} = \left(\dot{m}_{\mathrm{W,in}} - \dot{m}_{\mathrm{W,rxn}}\right) + \left(\dot{m}_{\mathrm{P,in}} + \dot{m}_{\mathrm{P,rxn}}\right) \qquad \text{Equation 5}$$

Through substitution, we define the product mass fraction, x_P (Equation 6), as the total product mass divided by the total mass exiting the reaction zone as a function of total current, I, and inlet water volumetric sweep rate, Q.

$$x_{\mathrm{P}} = \frac{\dot{m}_{\mathrm{P,in}} + \dot{m}_{\mathrm{P,rxn}}}{\dot{m}_{\mathrm{out}}} = \frac{\dot{m}_{\mathrm{P,in}} + \frac{I}{z_{\mathrm{P}} F} MW_{\mathrm{P}}}{\left(\rho_{\mathrm{W}} Q - \frac{I}{z_{\mathrm{W}} F} MW_{\mathrm{W}}\right) + \left(\dot{m}_{\mathrm{P,in}} + \frac{I}{z_{\mathrm{P}} F} MW_{\mathrm{P}}\right)} \qquad \text{Equation 6}$$

Here, I can either represent a partial current towards a target product or, assuming 100% faradaic efficiency, a total current. The water mass fraction, x_W (Equation 7), is readily determined from x_P because we assume a binary mixture in the liquid phase.

$$x_W = 1 - x_P \qquad \text{Equation 7}$$

Each cathodic half reaction consumes CO_2, H_2O, and electrons and produces hydrogenated products and OH^- as shown in **Table 1**. Included are the relevant stoichiometric constants—n_P (the number of moles of CO_2 per mole of product), z_P, and z_W—as well as the product molecular weights, MW_P. We convert from a mole to mass basis because it can be more convenient to work with mass (or weight) fractions at high solute concentrations.

Table 1 CO2R half-reaction stoichiometry for liquid products

Half reaction	n_P	z_P	z_W	MW_P (g/mol)
$CO_2 + 2e^- + H_2O \rightarrow \boldsymbol{HCOO^-} + OH^-$	1	2	2	46.03
$CO_2 + 6e^- + 5H_2O \rightarrow \boldsymbol{CH_3OH} + 6OH^-$	1	6	6/5	32.04
$2CO_2 + 12e^- + 9H_2O \rightarrow \boldsymbol{C_2H_5OH} + 12OH^-$	2	12	12/9	46.07
$3CO_2 + 18e^- + 13H_2O \rightarrow \boldsymbol{C_3H_7OH} + 18OH^-$	3	18	18/13	60.09

This simple mass balance analysis enables consideration of the cumulative impact of water consumption and organic product generation on the physical properties of the solution and the wettability of the electrode. Note that the stoichiometric constants only account for the *half-reaction* water balances at the *cathode*, as the microenvironment local to the electrode-electrolyte interface will determine flooding. However, in the full cell, water is generated at the anode, which, depending on the cathode chemistry, offsets some or all of the water consumption (**Table S4**, Supporting Information). For example, there is no net water consumed for the conversion of CO_2 to formate/FA, but CO_2 to alcohols reactions still require net water consumption.

We construct composition contour plots for FA, MeOH, EtOH, and PrOH (**Fig. 5**) by calculating x_P across many currents and flow rates. The y-axes are reported on a log scale for clarity across several magnitudes of flow rates. Product composition isoclines reported in % by mass (solid lines) start at the 0.1, 1, and 10% and then continue from 10–100% in increments of 10%. Sweeping the

current from 0–1000 mA at fixed Q results in a linear increase in the production rate (Equation 2), while increasing Q from 0.001–1 mL min^{-1} at fixed I decreases x_P due to their inverse relation. The composition contours generally shift downward with deeper reduction products and increasing molecular weight, with an exception of FA that has similar molecular weight to EtOH. FA composition is less sensitive to Q at fixed I, whereas the alcohols are more likely to reach high concentration through modest changes to Q.

Determining 90°-crossover compositions from *ex situ* contact angle data allows us to estimate a *best-case scenario* condition that may lead to a sign change, from positive to negative, in P_C. We use wettability metrics for PTFE to represent GDE stability because it is assumed to be invariant to mild voltage biases to the electrode. In contrast, graphite is the more polarizable GDE component, so we may anticipate that its wettability will increase as a function of electrode voltage according to electrowetting phenomena [53,54]. The measured crossover composition, here, corresponding to a measured 90° contact angle on PTFE, is indicated with a black dot-dash line for each of the product subpanels in **Fig. 5**. These crossover compositions were determined by interpolating between measured data points (**Fig. S4**, Supporting Information). If making predictions using a Zisman rule, all liquids with γ below that of a crossover value, which is either 47 mN/m (⋯, this work) or 40 mN/m (---, Zisman), should wet PTFE with a contact angle less than 90°. We estimate the crossover composition for each CO2R product by finding the water composition at which the γ curves (**Fig. S2b**, Supporting Information) reach the 90°-threshold. While there are discrepancies between the measurements and predicted isoclines, the differences between the operating conditions needed to achieve each composition are relatively minor. At flow rates above each crossover line, the sweep stream provides enough water to the reaction zone at a given current to keep the product composition below the critical imbibition point. Put another way, for a given sweep rate, the electrochemical conversion rate is slow enough that enrichment of organic species in the reaction zone is not so great as to lead to flooding.

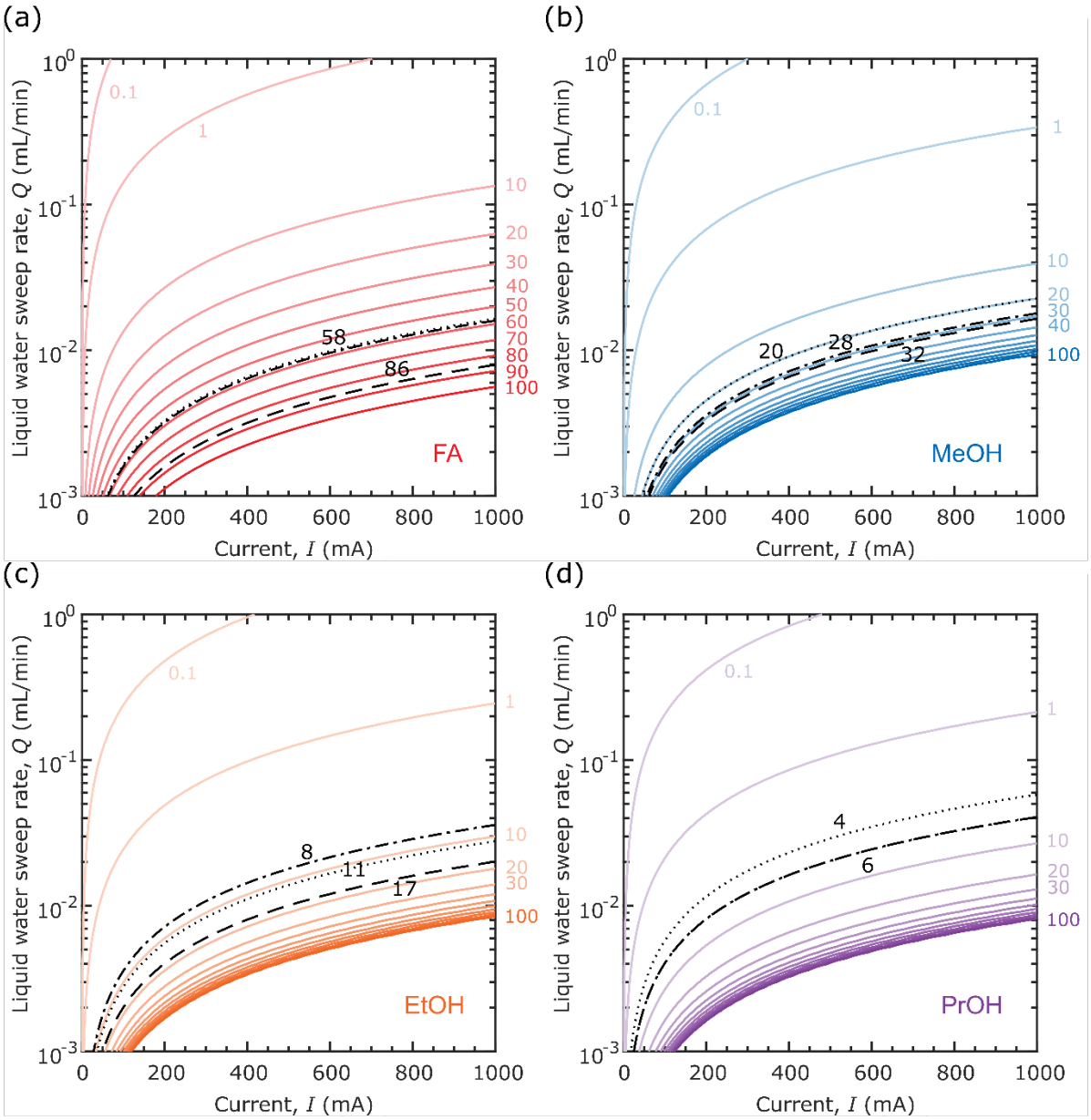

Fig. 5 The liquid product concentration, x_W, reported in percentage by mass with the solid contours, is calculated for (a) FA, (b) MeOH, (c) EtOH, and (d) PrOH as a function of liquid inlet water flow rate and current by using a mass balance around a hypothetical CO_2 electrolyzer with a flowing electrolyte stream. The additional black dashed lines correspond to the measured (·-) and theoretically-predicted (··· 47 mN/m from this work; ---, 40 mN/m from Zisman) $\theta = 90°$ point on PTFE at which the mixture transitions from non-wetting to wetting.

In agreement with the contact angle measurements, the ordering and position of the crossover composition isoclines in *Q-I* space align with the γ and polarity of the organic species (**Fig. S2b**, Supporting Information). Plotting the isoclines for different liquid species together (**Fig. 6**) is an

effective way for determining if electrolyzer operating conditions need to be tailored according to product identity. For example, although FA mixtures wet at much high concentrations as compared to the alcohol mixtures, the operating conditions required to reach the crossover points are similar for species of equivalent polarity. At the extremes of species wettability (i.e., PrOH versus FA), however, the Q required to induce contact angle crossover varies by nearly an order of magnitude at the same I.

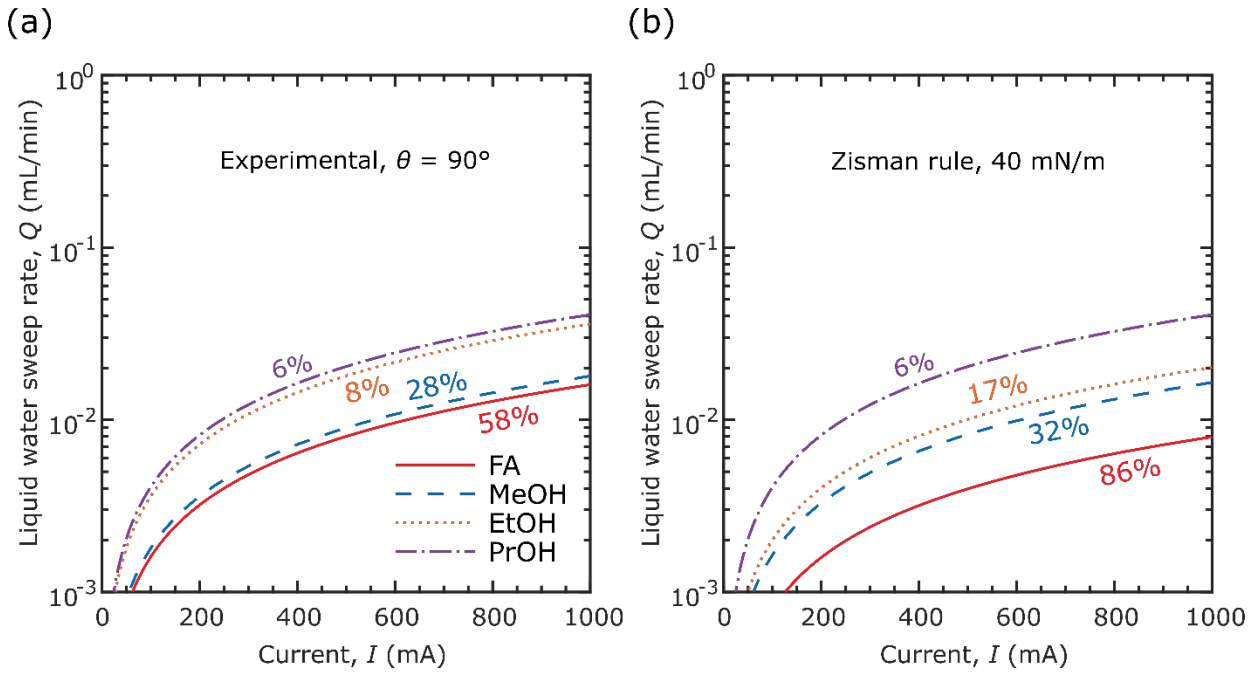

Fig. 6 Crossover composition contours correspond to $\theta = 90°$ on PTFE (when $P_C = 0$ bar) as (a) measured in this work and (b) predicted from a Zisman rule surface tension threshold ($\theta = 90°$) of 40 mN/m for nonpolar solvents on PTFE.

Now with x_P mapped to different operating conditions, we can connect the wettability of the various liquid mixtures to a simple prediction of P_C using Equation 1, which is necessary for understanding the pressure differentials required to maintain a stable gas-liquid interface in a gas-fed CO_2 electrolyzer. Again, here we do not consider complex physical and geometric features evident in real GDE materials (thickness, pore size distribution, fibers spacing, particles sizes, mixed wettability) [55,56] to determine P_C because simplified models such Young-Laplace are able to capture general capillarity trends. However, further analyses explicitly considering saturation or wetting dynamics in electrodes with finite volume could expand from these zeroth-order analyses of interfacial P_C to refine predictions of stable operating envelopes. We first compute P_C at various levels of water content, x_W (**Fig. 7**). The data associated with this figure are

reported in **Table S5** in the Supporting Information. We employ interpolated PTFE contact angle values (**Fig. S4**) to calculate P_C with a radius, r, of 0.1 μm as representative of the effective pore radius for expanded PTFE membranes (e.g., Porex PM21M) similar to those used as GDE scaffolds in recent work [24]. We next overlay the P_C values corresponding to each x_P contour (**Fig. 8**) to convert the composition map into one for predicting differential pressure thresholds. The P_C isoclines can be thought of as an estimation of the magnitude of the maximum liquid-gas overpressure that a GDE could withstand while still maintaining interfacial stability / avoiding flooding. Comparing the operating envelope for each liquid-PTFE combination as a function of current and flow rate is useful for predicting if any notable physical changes to the system equilibrium emerge when targeting different CO2R products. By comparing the location of the critical isoclines (where $P_C = 0$) in Q-I space, we observe ordering in agreement with the relative wettability (PrOH > EtOH > MeOH > FA) as determined from contact angle measurements. The critical composition lines generally shift upward from FA to PrOH, according to chain length, depth of electroreduction, and decreasing polarity, which taken together indicate that the allowable operating space will narrow as the deeper CO2R products considered in this subset are pursued.

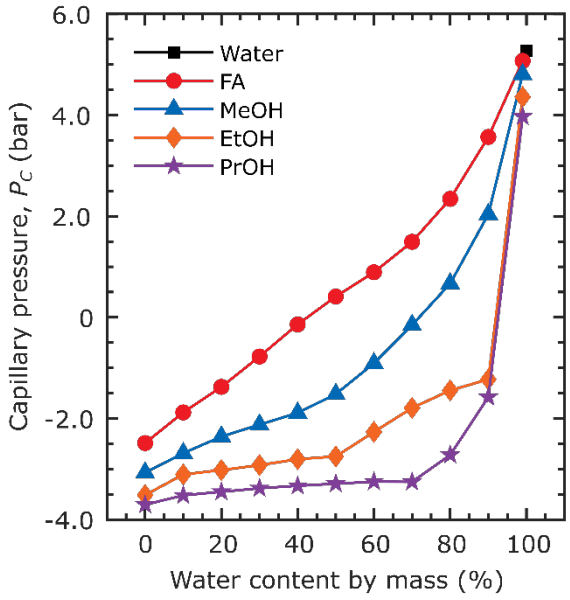

Fig. 7 Capillary pressure, P_C, plotted as a function of water content by mass, x_W, and CO2R liquid product.

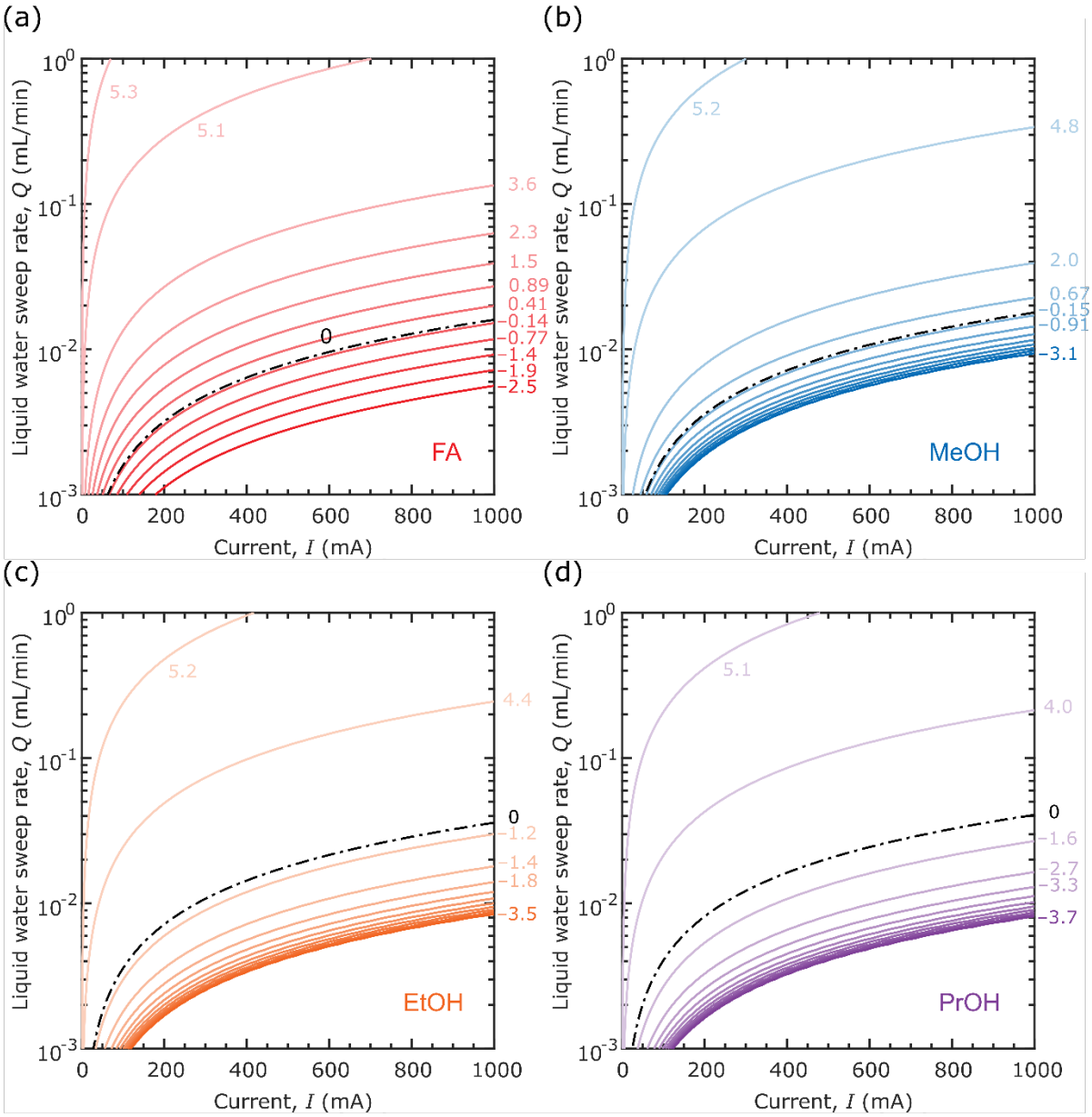

Fig. 8 Capillary pressure, P_C, (bar) calculated for a pore radius, *r,* of 0.2 μm is overlaid onto the contours corresponding to the product compositions, x_P, shown in **Fig. 5** as a function of liquid sweep rate, Q, and current, I. The crossover contours, at which $P_C = 0$ bar, are indicated by the black dashed lines.

These predictions suggest that the operating envelope for FA is likely to be wider than for alcohols for PTFE-supported GDEs. However, when considering that many existing industrial GDEs are composite materials (conductive metal and hydrophobic PTFE components) with mixed wettability properties (*vide supra*, oxygen depolarized cathodes), these contours may constitute the *best possible* set of conditions correlating to P_C crossover. Using composite GDEs may

ultimately prove necessary when scaling to larger cell areas due to enhanced through-plane conductivity as compared to the PTFE-supported electrodes. Despite the increased flooding risk imparted to GDEs by imbuing them with conductive additives, there are still opportunities for targeted tuning wet-proofing content in porous media to achieve both favorable P_C envelopes [57] as well as high CO2R activity and faradaic efficiency [8,45].

4. Opportunities for the integration of oleophobic materials

Oleophobic treatments constitute a readily-available modification to GDEs that may better suit aqueous-organic environments [30]. Introducing oleophobicity to PTFE sheets has enabled their use as venting materials in electronic devices such as in batteries and other electronics filled with organic solvents [58]. Although measuring the intrinsic wettability of rough or porous materials with macroscopic sessile drop methods, we can still compare the relative effectiveness of modifying the PTFE surface. Using the same methods as described before for solid PTFE (*vide supra*), we measured the apparent contact angles (**Fig. 9**) of the test liquids on two different porous sheets, expanded PTFE (PM21M, Porex) and sintered oleophobic PTFE (PMV15T, Porex) sheets. The raw data are reported in **Tables S6** and **S7** of the Supporting Information. The non-wetting envelope ($\theta > 90°$) for all of the test liquids is expanded for the porous materials as compared to the dense, flat PTFE sheet shown in **Fig. 2**. As mentioned earlier, surface roughness and entrapped gases can increase the apparent phobicity/philicity of a given solid-liquid combination. However, while the porous PTFE membrane is ultimately wetted by lower surface tension mixtures, the oleophobic membrane does not exhibit any $\theta < 90°$. These initial results demonstrate that appropriate modifications to extant and proven material sets may greatly improve the wettability characteristics. While the oleophobic treatment here was applied to a PTFE substrate, in principle, it could be expanded to other polymers, metals, or carbon substrates to improve liquid repellency or tune wettability.

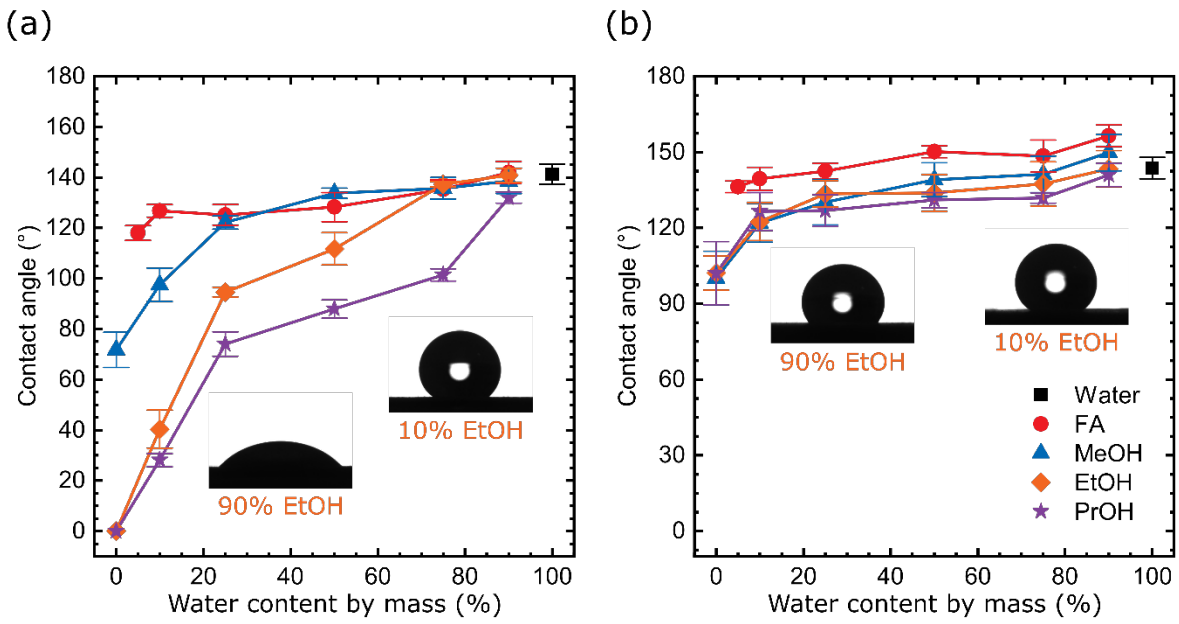

Fig. 9 Apparent sessile drop contact angles for selected CO2R product liquids as a function of water content by mass on (a) Porex PM21M expanded PTFE and (b) Porex PMV15T oleophobic treated sintered PTFE sheet.

5. Outlook

The generation of concentrated liquid products at CO_2 electrolyzer outlets is an economically attractive operating objective (*vide supra*) that may be attainable by targeting high current to liquid sweep rate ratios. Investigating these conditions through the use of a simple mass balance model, in combination with *ex situ* contact angle measurements, enables simulation of the local environment at the cathode-electrolyte interface and the propensity of GDE flooding due to enrichment by organic products. Such critical compositions are illustrated in contour plots enabling connections between cell operating conditions (liquid sweep rate and applied currents) and electrode properties (wettability). Such estimations of electrode flooding enable us to predict that FA-generating electrolysis cells should be more stable than the equivalent alcohol-producing cells when targeting high-mass-fraction effluents. We also see an opportunity to leverage existing surface modification technologies to augment the wettability characteristics of current GDE material sets, possibly with oleophobic treatments, towards the goal of expanding the stable operating envelope for CO_2-to-alcohols electrolyzers. Through this exploration of some of the material challenges that face CO2R during the necessary scale-up phase, we hope to inspire

additional researchers in this field to consider these obstacles at an early stage of technology development.

Conflict of Interest

We wish to confirm that there are no known conflicts of interest associated with this publication and there has been no significant financial support for this work that could have influenced its outcome.

CRediT author statement

McLain E. Leonard: Conceptualization, Methodology, Formal Analysis, Investigation, Resources, Writing – Original Draft, Writing – Review & Editing, Visualization **Michael J. Orella:** Methodology, Software, Writing – Original Draft, Writing – Review & Editing **Nick Aiello:** Investigation **Antoni Forner-Cuenca** Methodology, Formal Analysis, Writing – Review & Editing **Yuriy Román-Leshkov:** Supervision **Fikile R. Brushett:** Funding Acquisition, Project Administration, Supervision, Writing – Review & Editing

Acknowledgements

The authors acknowledge the financial support of DOE SBIR Contract #DE-SC0015173. The authors kindly thank the members of the Gleason Group and Prof. Karen Gleason for supporting us as we used their goniometer system to measure contact angles. The authors also thank Lauren E. Clarke and Charles T.-C. Wan of the Brushett Research Group for insightful discussions.

References

[1] W.A. Smith, T. Burdyny, D.A. Vermaas, H. Geerlings, Pathways to Industrial-Scale Fuel Out of Thin Air from CO2 Electrolysis, Joule. 0 (2019). https://doi.org/10.1016/j.joule.2019.07.009.

[2] R.M. Darling, K.G. Gallagher, J.A. Kowalski, S. Ha, F.R. Brushett, Pathways to low-cost electrochemical energy storage: a comparison of aqueous and nonaqueous flow batteries, Energy Environ. Sci. 7 (2014) 3459–3477. https://doi.org/10.1039/C4EE02158D.

[3] P.D. Luna, C. Hahn, D. Higgins, S.A. Jaffer, T.F. Jaramillo, E.H. Sargent, What would it take for renewably powered electrosynthesis to displace petrochemical processes?, Science. 364 (2019) eaav3506. https://doi.org/10.1126/science.aav3506.

[4] Y. Hori, Electrochemical CO2 reduction on metal electrodes, in: Modern Aspects of Electrochemistry, Springer, 2008: pp. 89–189. http://link.springer.com/chapter/10.1007/978-0-387-49489-0_3 (accessed January 25, 2016).

[5] J.T. Feaster, C. Shi, E.R. Cave, T. Hatsukade, D.N. Abram, K.P. Kuhl, C. Hahn, J.K. Nørskov, T.F. Jaramillo, Understanding Selectivity for the Electrochemical Reduction of Carbon Dioxide to Formic Acid and Carbon Monoxide on Metal Electrodes, ACS Catal. (2017) 4822–4827. https://doi.org/10.1021/acscatal.7b00687.

[6] S. Ringe, E.L. Clark, J. Resasco, A. Walton, B. Seger, A.T. Bell, K. Chan, Understanding cation effects in electrochemical CO2 reduction, Energy Environ. Sci. (2019). https://doi.org/10.1039/C9EE01341E.

[7] P. Lobaccaro, M.R. Singh, E.L. Clark, Y. Kwon, A.T. Bell, J.W. Ager, Effects of temperature and gas–liquid mass transfer on the operation of small electrochemical cells for the quantitative evaluation of CO2 reduction electrocatalysts, Phys. Chem. Chem. Phys. 18 (2016) 26777–26785. https://doi.org/10.1039/C6CP05287H.

[8] L.-C. Weng, A.T. Bell, A.Z. Weber, Modeling gas-diffusion electrodes for CO2 reduction, Phys. Chem. Chem. Phys. 20 (2018) 16973–16984. https://doi.org/10.1039/C8CP01319E.

[9] T. Burdyny, W.A. Smith, CO2 reduction on gas-diffusion electrodes and why catalytic performance must be assessed at commercially-relevant conditions, Energy Environ. Sci. 12 (2019) 1442–1453. https://doi.org/10.1039/C8EE03134G.

[10] M.R. Thorson, K.I. Siil, P.J.A. Kenis, Effect of Cations on the Electrochemical Conversion of CO2 to CO, J. Electrochem. Soc. 160 (2013) F69–F74. https://doi.org/10.1149/2.052301jes.

[11] B. Kim, F. Hillman, M. Ariyoshi, S. Fujikawa, P.J.A. Kenis, Effects of composition of the micro porous layer and the substrate on performance in the electrochemical reduction of CO2 to CO, Journal of Power Sources. 312 (2016) 192–198. https://doi.org/10.1016/j.jpowsour.2016.02.043.

[12] C. Chen, J.F. Khosrowabadi Kotyk, S.W. Sheehan, Progress toward Commercial Application of Electrochemical Carbon Dioxide Reduction, Chem. 4 (2018) 2571–2586. https://doi.org/10.1016/j.chempr.2018.08.019.

[13] G.O. Larrazábal, P. Strøm-Hansen, J.P. Heli, K. Zeiter, K.T. Therkildsen, I. Chorkendorff, B. Seger, Analysis of Mass Flows and Membrane Cross-over in CO2 Reduction at High Current Densities in an MEA-Type Electrolyzer, ACS Appl. Mater. Interfaces. 11 (2019) 41281–41288. https://doi.org/10.1021/acsami.9b13081.

[14] Z. Yin, H. Peng, X. Wei, H. Zhou, J. Gong, M. Huai, L. Xiao, G. Wang, J. Lu, L. Zhuang, An alkaline polymer electrolyte CO2 electrolyzer operated with pure water, Energy Environ. Sci. 12 (2019) 2455–2462. https://doi.org/10.1039/C9EE01204D.
[15] Z. Liu, H. Yang, R. Kutz, R.I. Masel, CO $_2$ Electrolysis to CO and O $_2$ at High Selectivity, Stability and Efficiency Using Sustainion Membranes, Journal of The Electrochemical Society. 165 (2018) J3371–J3377. https://doi.org/10.1149/2.0501815jes.
[16] H.S. Fogler, Elements of Chemical Reaction Engineering, 4th ed., Prentice Hall, 2006.
[17] M.J. Orella, S.M. Brown, M.E. Leonard, Y. Román-Leshkov, F.R. Brushett, A General Technoeconomic Model for Evaluating Emerging Electrolytic Processes, Energy Technology. n/a (n.d.) 1900994. https://doi.org/10.1002/ente.201900994.
[18] F.P.G. de Arquer, C.-T. Dinh, A. Ozden, J. Wicks, C. McCallum, A.R. Kirmani, D.-H. Nam, C. Gabardo, A. Seifitokaldani, X. Wang, Y.C. Li, F. Li, J. Edwards, L.J. Richter, S.J. Thorpe, D. Sinton, E.H. Sargent, CO2 electrolysis to multicarbon products at activities greater than 1 A cm−2, Science. 367 (2020) 661–666. https://doi.org/10.1126/science.aay4217.
[19] B. Endrődi, E. Kecsenovity, A. Samu, F. Darvas, R.V. Jones, V. Török, A. Danyi, C. Janáky, Multilayer Electrolyzer Stack Converts Carbon Dioxide to Gas Products at High Pressure with High Efficiency, ACS Energy Lett. 4 (2019) 1770–1777. https://doi.org/10.1021/acsenergylett.9b01142.
[20] H. Yang, J.J. Kaczur, S.D. Sajjad, R.I. Masel, Electrochemical conversion of CO 2 to formic acid utilizing Sustainion^{TM} membranes, Journal of CO2 Utilization. 20 (2017) 208–217. https://doi.org/10.1016/j.jcou.2017.04.011.
[21] C.M. Gabardo, C.P. O'Brien, J.P. Edwards, C. McCallum, Y. Xu, C.-T. Dinh, J. Li, E.H. Sargent, D. Sinton, Continuous Carbon Dioxide Electroreduction to Concentrated Multi-carbon Products Using a Membrane Electrode Assembly, Joule. (2019). https://doi.org/10.1016/j.joule.2019.07.021.
[22] D.S. Ripatti, T.R. Veltman, M.W. Kanan, Carbon Monoxide Gas Diffusion Electrolysis that Produces Concentrated C2 Products with High Single-Pass Conversion, Joule. 3 (2019) 240–256. https://doi.org/10.1016/j.joule.2018.10.007.
[23] C.-T. Dinh, F.P. García de Arquer, D. Sinton, E.H. Sargent, High Rate, Selective, and Stable Electroreduction of CO2 to CO in Basic and Neutral Media, ACS Energy Lett. 3 (2018) 2835–2840. https://doi.org/10.1021/acsenergylett.8b01734.
[24] C.-T. Dinh, T. Burdyny, M.G. Kibria, A. Seifitokaldani, C.M. Gabardo, F.P.G. de Arquer, A. Kiani, J.P. Edwards, P.D. Luna, O.S. Bushuyev, C. Zou, R. Quintero-Bermudez, Y. Pang, D. Sinton, E.H. Sargent, CO2 electroreduction to ethylene via hydroxide-mediated copper catalysis at an abrupt interface, Science. 360 (2018) 783–787. https://doi.org/10.1126/science.aas9100.
[25] W. Vielstich, A. Lamm, H.A. Gasteiger, eds., Handbook of Fuel Cells : Fundamentals, Technology, and Applications, Wiley, 2003. https://lib.mit.edu/record/cat00916a/mit.001126960 (accessed February 13, 2020).
[26] S. Pinnow, N. Chavan, T. Turek, Thin-film flooded agglomerate model for silver-based oxygen depolarized cathodes, J Appl Electrochem. 41 (2011) 1053–1064. https://doi.org/10.1007/s10800-011-0311-2.
[27] T. Haas, R. Krause, R. Weber, M. Demler, G. Schmid, Technical photosynthesis involving CO 2 electrolysis and fermentation, Nature Catalysis. 1 (2018) 32–39. https://doi.org/10.1038/s41929-017-0005-1.
[28] W.M. Deen, Analysis of Transport Phenomena, 2nd ed., Oxford University Press, 2011.

[29] P.-G. de Gennes, F. Brochard-Wyart, D. Quéré, Capillarity and Wetting Phenomena: Drops, Bubbles, Pearls, Waves, Springer, New York, NY, 2010.
[30] W.A. ZISMAN, Relation of the Equilibrium Contact Angle to Liquid and Solid Constitution, in: Contact Angle, Wettability, and Adhesion, AMERICAN CHEMICAL SOCIETY, 1964: pp. 1–51. https://doi.org/10.1021/ba-1964-0043.ch001.
[31] T. Young, III. An essay on the cohesion of fluids, Phil. Trans. R. Soc. Lond. 95 (1805) 65–87. https://doi.org/10.1098/rstl.1805.0005.
[32] R.N. Wenzel, RESISTANCE OF SOLID SURFACES TO WETTING BY WATER, Ind. Eng. Chem. 28 (1936) 988–994. https://doi.org/10.1021/ie50320a024.
[33] A.B.D. Cassie, S. Baxter, Wettability of porous surfaces, Transactions of the Faraday Society. 40 (1944) 546. https://doi.org/10.1039/tf9444000546.
[34] ISO 4920:2012, Textile fabrics — Determination of resistance to surface wetting (spray test), International Organization for Standardization, Geneva, Switzerland, 2012. https://www.iso.org/standard/50706.html.
[35] ISO 9073-17:2008, Textiles — Test methods for nonwovens — Part 17: Determination of water penetration (spray impact), International Organization for Standardization, Geneva, Switzerland, 2008. https://www.iso.org/standard/42095.html.
[36] M.J. Orella, DropPy, 2020. https://github.com/michaelorella/droppy.
[37] J.R. Rumble, ed., CRC Handbook of Chemistry and Physics, 99th Edition, CRC Press/Taylor & Francis, Boca Raton, FL, 2018.
[38] A. Kozbial, C. Trouba, H. Liu, L. Li, Characterization of the Intrinsic Water Wettability of Graphite Using Contact Angle Measurements: Effect of Defects on Static and Dynamic Contact Angles, Langmuir. 33 (2017) 959–967. https://doi.org/10.1021/acs.langmuir.6b04193.
[39] C. Delacourt, P.L. Ridgway, J.B. Kerr, J. Newman, Design of an Electrochemical Cell Making Syngas (CO+H[sub 2]) from CO[sub 2] and H[sub 2]O Reduction at Room Temperature, Journal of The Electrochemical Society. 155 (2008) B42. https://doi.org/10.1149/1.2801871.
[40] M.S. Naughton, F.R. Brushett, P.J.A. Kenis, Carbonate resilience of flowing electrolyte-based alkaline fuel cells, Journal of Power Sources. 196 (2011) 1762–1768. https://doi.org/10.1016/j.jpowsour.2010.09.114.
[41] F.R. Brushett, M.S. Naughton, J.W.D. Ng, L. Yin, P.J.A. Kenis, Analysis of Pt/C electrode performance in a flowing-electrolyte alkaline fuel cell, International Journal of Hydrogen Energy. 37 (2012) 2559–2570. https://doi.org/10.1016/j.ijhydene.2011.10.078.
[42] M.S. Naughton, G.H. Gu, A.A. Moradia, P.J.A. Kenis, Tailoring electrode hydrophobicity to improve anode performance in alkaline media, Journal of Power Sources. 242 (2013) 581–588. https://doi.org/10.1016/j.jpowsour.2013.05.054.
[43] K. Wu, E. Birgersson, B. Kim, P.J.A. Kenis, I.A. Karimi, Modeling and Experimental Validation of Electrochemical Reduction of CO2 to CO in a Microfluidic Cell, J. Electrochem. Soc. 162 (2015) F23–F32. https://doi.org/10.1149/2.1021414jes.
[44] S. Verma, X. Lu, S. Ma, R.I. Masel, P.J.A. Kenis, The effect of electrolyte composition on the electroreduction of CO2 to CO on Ag based gas diffusion electrodes, Phys. Chem. Chem. Phys. 18 (2016) 7075–7084. https://doi.org/10.1039/C5CP05665A.
[45] B. Kim, F. Hillman, M. Ariyoshi, S. Fujikawa, P.J.A. Kenis, Effects of composition of the micro porous layer and the substrate on performance in the electrochemical reduction of CO2

to CO, Journal of Power Sources. 312 (2016) 192–198. https://doi.org/10.1016/j.jpowsour.2016.02.043.
[46] S. Verma, Y. Hamasaki, C. Kim, W. Huang, S. Lu, H.-R.M. Jhong, A.A. Gewirth, T. Fujigaya, N. Nakashima, P.J.A. Kenis, Insights into the Low Overpotential Electroreduction of CO2 to CO on a Supported Gold Catalyst in an Alkaline Flow Electrolyzer, ACS Energy Lett. 3 (2018) 193–198. https://doi.org/10.1021/acsenergylett.7b01096.
[47] K. Liu, W.A. Smith, T. Burdyny, Introductory Guide to Assembling and Operating Gas Diffusion Electrodes for Electrochemical CO2 Reduction, ACS Energy Lett. (2019) 639–643. https://doi.org/10.1021/acsenergylett.9b00137.
[48] C.M. Gabardo, A. Seifitokaldani, J.P. Edwards, C.-T. Dinh, T. Burdyny, M.G. Kibria, C.P. O'Brien, E.H. Sargent, D. Sinton, Combined high alkalinity and pressurization enable efficient CO2 electroreduction to CO, Energy Environ. Sci. 11 (2018) 2531–2539. https://doi.org/10.1039/C8EE01684D.
[49] D. Salvatore, C.P. Berlinguette, Voltage Matters When Reducing CO2 in an Electrochemical Flow Cell, ACS Energy Lett. (2019) 215–220. https://doi.org/10.1021/acsenergylett.9b02356.
[50] Y. Xu, J.P. Edwards, J. Zhong, C.P. O'Brien, C.M. Gabardo, C. McCallum, J. Li, C.-T. Dinh, E.H. Sargent, D. Sinton, Oxygen-tolerant electroproduction of C2 products from simulated flue gas, Energy Environ. Sci. (2019). https://doi.org/10.1039/C9EE03077H.
[51] J.P. Edwards, Y. Xu, C.M. Gabardo, C.-T. Dinh, J. Li, Z. Qi, A. Ozden, E.H. Sargent, D. Sinton, Efficient electrocatalytic conversion of carbon dioxide in a low-resistance pressurized alkaline electrolyzer, Applied Energy. 261 (2020) 114305. https://doi.org/10.1016/j.apenergy.2019.114305.
[52] K.G. Schulz, U. Riebesell, B. Rost, S. Thoms, R.E. Zeebe, Determination of the rate constants for the carbon dioxide to bicarbonate inter-conversion in pH-buffered seawater systems, Marine Chemistry. 100 (2006) 53–65. https://doi.org/10.1016/j.marchem.2005.11.001.
[53] A. Kutana, K.P. Giapis, Atomistic Simulations of Electrowetting in Carbon Nanotubes, Nano Lett. 6 (2006) 656–661. https://doi.org/10.1021/nl052393b.
[54] D. J. Lomax, P. Kant, A. T. Williams, H. V. Patten, Y. Zou, A. Juel, R.A. W. Dryfe, Ultra-low voltage electrowetting using graphite surfaces, Soft Matter. 12 (2016) 8798–8804. https://doi.org/10.1039/C6SM01565D.
[55] W.R. Purcell, Interpretation of Capillary Pressure Data, Journal of Petroleum Technology. 2 (1950) 11–12. https://doi.org/10.2118/950369-G.
[56] A. Forner-Cuenca, J. Biesdorf, A. Lamibrac, V. Manzi-Orezzoli, F.N. Büchi, L. Gubler, T.J. Schmidt, P. Boillat, Advanced Water Management in PEFCs: Diffusion Layers with Patterned Wettability II. Measurement of Capillary Pressure Characteristic with Neutron and Synchrotron Imaging, Journal of The Electrochemical Society. 163 (2016) F1038–F1048.
[57] J.T. Gostick, M.A. Ioannidis, M.W. Fowler, M.D. Pritzker, Wettability and capillary behavior of fibrous gas diffusion media for polymer electrolyte membrane fuel cells, Journal of Power Sources. 194 (2009) 433–444. https://doi.org/10.1016/j.jpowsour.2009.04.052.
[58] Virtek IP-rated PTFE vents | sintered PTFE material | sealed enclosures, Porex. (n.d.). https://www.porex.com/markets/electronics/ip-rated-protection-vents/ (accessed February 29, 2020).